LETTER

Ultrafast spin polarization in a multiferroic manganite $BiFe_{0.5}Mn_{0.5}O_3$ thin film

To cite this article: Z. Y. Zhang *et al* 2015 *EPL* **112** 37007

A Letters Journal Exploring the Frontiers of Physics

November 2015

EPL, **112** (2015) 37007 www.epljournal.org
doi: 10.1209/0295-5075/112/37007

Ultrafast spin polarization in a multiferroic manganite $BiFe_{0.5}Mn_{0.5}O_3$ thin film

Z. Y. Zhang[1], Z. M. Jin[1(a)], X. Lin[1], Z. X. Cheng[2], H. Y. Zhao[3], H. Kimura[4] and G. H. Ma[1(b)]

[1] *Department of Physics, Shanghai University - Shanghai 200444, China*
[2] *Institute for Superconducting and Electronic Materials, University of Wollongong - New South Wales 2500, Australia*
[3] *Department of Materials Science and Engineering, Wuhan Institute of Technology - 693 Xiongchu Road, Wuhan 430073, China*
[4] *National Institute for Materials Science - Sengen 1-2-1, Tsukuba, Ibaraki 305-0047, Japan*

received 23 September 2015; accepted in final form 2 November 2015
published online 25 November 2015

PACS 78.47.J- – Ultrafast spectroscopy (< 1 ps)
PACS 78.20.-e – Optical properties of bulk materials and thin films
PACS 75.47.Lx – Magnetic oxides

Abstract – In this work, we present observations of ultrafast carrier dynamics and spin polarization in a multiferroic manganite $BiFe_{0.5}Mn_{0.5}O_3$ film excited by linearly and circularly polarized femtosecond pulses, respectively. The *d*-band charge transfer transition is reasonably assigned to $\Gamma_3 \rightarrow \Gamma_5$. The transient reflectivity decay on a time scale as fast as only 0.3 ps is consistent with the picture of ultrafast electron-phonon coupling. The ultrafast switching of polarization ellipticity (< 150 fs) originates from a transient coherent spin polarization by optical orientation. The ultrafast spin polarization switching is assigned to the Raman coherence process.

Introduction. – Multiferroic materials, which show the simultaneous coexistence of ferroelectric and magnetic phases, have attracted extensive attention in the past several decades [1–3]. By doping another magnetic transition metal cation on the B-site in a ABO_3 perovskite oxide to create a double perovskite oxide can provide ferromagnetic exchange according to the Goodenough-Kanamori rules [4]. The multiferroic manganite $BiFe_{0.5}Mn_{0.5}O_3$ (BFMO), a compound of $BiFeO_3$ and $BiMnO_3$, has been recently designed theoretically and fabricated experimentally. More intense research has resulted in promising findings on BFMO such as multiferroicity coexisting with a small net ferromagnetic magnetization at room temperature and ferroelectricity at low temperature [5–7]. In the previous work, based on the small magnetic moment observed in *M-H* loops, Mn-O-Mn was found to be antiferromagnetically ordered in BFMO [8]. It is important to note that the desired electronic configuration of B-B′ cations is difficult to obtain, owing to the mixed valence states. Furthermore, long-range ferromagnetism requires alternating B-B′ cation ordering along the fundamental perovskite directions [4].

Femtosecond optical pump pulses have been widely used to suddenly create a nonequilibrium state in semiconductors [9,10] and ferromagnetic materials [11,12]. The subsequent electron and/or spin relaxation dynamics is measured by a time-delayed probe pulse. Based on the transfer of angular momentum from circularly polarized light to the medium, nonequilibrium electron polarization was created in antiferromagnetic Mott insulators [13], topological insulators [14], and also paramagnetic crystals [15], which has been ascribed to a transient spin polarization with fast depolarization. A less studied and very interesting material system is that of the multiferroics, which are generally classified as strongly correlated electron systems, combining both magnetic and semiconducting properties. In recent years, optical pump-probe spectroscopy has been employed as a crucial alternative tool for investigating the strong coupling between spin, charge, and the lattice on different time scales in multiferroic systems [16–20]. In addition, the individual degrees of freedom are sensitive to various optical characterizations of the probe pulse, such as absorption, reflection, or polarization. The present work is motivated by discovering the answer to the question of whether it is possible to generate a coherent transient spin polarization in a multiferroic system by using ultrashort laser pulses.

(a) E-mail: physics_izm@shu.edu.cn
(b) E-mail: ghma@staff.shu.edu.cn

Experimental details. – A well-crystallized single-phase BFMO film was deposited on a silicon substrate using the pulsed laser deposition method (PLD) at 923 K with 500–600 mtorr dynamic oxygen. The film thickness is about 150 nm. A time-resolved pump-probe study of the BFMO film was measured with a standard reflection geometry. The light source was provided by a commercial mode-locked Ti: sapphire laser (Spitfire Pro, Spectra-Physics) running at the repetition rate of 1 kHz, with pulse width of 120 fs. A quarter wave plate was placed in the pump path, which enables the tuning of the pump pulse helicity between right and left circularly polarized states, with its fast axis at an angle Φ to the plane of the incident pump beam. Both the pump and the probe beams were focused on the surface of the sample with a spot diameter of about 200 μm. The fluence of the probe beam was weaker than that of the pump beam by at least a factor of ten. The BFMO film under investigation was photo-excited at 800 nm ($\equiv$ 1.55 eV). The penetration length is 100 nm for this system, which is much less than the thickness of the film under investigation here. Lock-in amplifier detection was used to record the pump-induced relative change in the reflected probe power as a function of the pump-probe delay time. In addition, a Glan prism and a balanced optical bridge were used to detect a pump-induced transient polarization rotation or ellipticity change of the linearly polarized probe beam. In our measurements, the sample was mounted in a closed-cycle liquid-He cryostat in a vacuum chamber with four optically accessible windows, which allowed control of the sample temperature in the range of 100–300 K.

Results and discussion. – Figure 1(a) shows the typical time-resolved transient reflectivity ($\Delta R/R$) of the BFMO film, which was measured with a pump fluence of 500 μJ/cm^2 at 120 K, also as a proof of the high quality of the BFMO film. During or immediately following the pulse, the $\Delta R/R$ starts rising sharply (population) and then decays by a nonradiative double exponential relaxation process. The fast and slow exponential decays mostly arise from the isotropic relaxations of non-equilibrium electron and lattice systems. We will find in the following that the electron dynamics is essentially slower than the coherent spin dynamics.

The photo-induced changes in the complex dielectric susceptibility that is driven by linearly and circularly polarized pump pulses correspond to linear and circular anisotropy, respectively [21]. The antisymmetric nonlinear perturbation of the dielectric permittivity tensor is deduced from the pump-induced magneto-optical (MO) Kerr effect. The ellipticity signal relates to $f(\tilde{n})\cdot\boldsymbol{M}$, where $\boldsymbol{M}$ is the magnetization, and $f(\tilde{n})$ is determined by the complex refractive index $\tilde{n}$ at the probe frequency. We can find the direct proportional relationship between $\boldsymbol{M}$ and the magnitude of the Gaussian-like peak in the ellipticity signal [9]. The symmetric nonlinear perturbation of the dielectric permittivity is deduced from the rotation of the

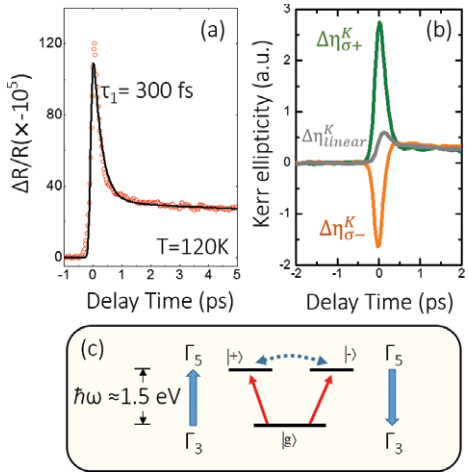

Fig. 1: (Color online) (a) The transient reflectivity at 120 K for the BFMO film. The points are the experimental data, and the solid line is a double exponential fitting of the data. (b) Typical photo-induced Kerr ellipticity responses to linearly polarized light ($\Delta\eta^K_{\rm linear}$), for right ($\Delta\eta^K_{\sigma+}$) and left ($\Delta\eta^K_{\sigma-}$) circularly polarized light pumping with zero external applied field, measured at room temperature. (c) Schematic energy-level diagram for the dipole allowed transition $\Gamma_3 \rightarrow \Gamma_5$ (solid arrows) between the hybridized $O^{2-}(2p)$-$Mn^{3+}(3d)$ state and the $Mn^{3+}(3d)$ states, (with $|g\rangle$ the ground state and $|+\rangle, |-\rangle$ the degenerate excited states).

probe polarization plane, which is due to the nonmagnetic, third-order nonlinear optical Kerr effect. It should be noted that only the off-diagonal elements of the complex dielectric susceptibility tensor are related to the spin-based phenomenon, which could be classified as the optical orientation (resonant case) [13] and the inverse Faraday effect (off-resonant case) [12,15].

The typical temporal behavior of the photo-induced polarization ellipticity of the reflected probe pulse ($\Delta\eta^K$) is shown in fig. 1(b), measured at room temperature, in which the excitations with linearly, and left- and right-circularly (σ_- and σ_+) polarized pump beams are used with a pump fluence of 8 mJ/cm^2 and a wavelength of 800 nm. A direct comparison of the time-resolved reflectivity and polarization ellipticity of the probe pulses has been performed to access the complete transient photo-induced phenomena in the sample. In contrast to the photo-induced reflectivity with a multi-exponential decay, the initial impression of the dynamical response $\Delta\eta^K_{\sigma+(-)}$ is a two-step recovery, which can be decomposed into a symmetric Gaussian peak and a relaxing slope. This striking difference in temporal profiles demonstrates a separate physical origin between the measured $\Delta\eta$ and the $\Delta R/R$ response. We note that the Gaussian-like peak of $\Delta\eta^K_{\sigma+(-)}$ remembers the polarization of the pump pulse, and it clearly changes sign when the helicity of the pump pulses is reversed. Moreover, $\Delta\eta^K_{\sigma+(-)}$ is at a maximum when the pump and probe beams overlap temporally. On the other hand, the measured slower relaxation slope is

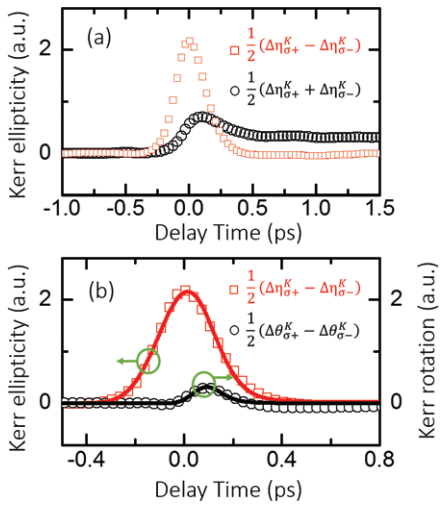

Fig. 2: (Color online) (a) The sum and difference of the transient ellipticity changes excited with right (σ_+) and left (σ_-) circularly polarized pump pulses. (b) Differences in the transient MO Kerr ellipticity and the rotation changes excited with opposite circularly polarized pump pulses, respectively. The solid lines are the fitted curves.

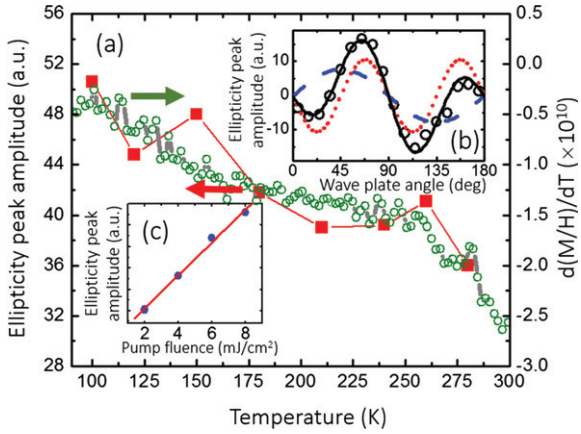

Fig. 3: (Color online) (a) The peak intensity of $1/2(\Delta\eta^K_{\sigma+} - \Delta\eta^K_{\sigma-})$ (red squares) and the $\mathrm{d}(M/H)/\mathrm{d}T$ curve (green circles) as a function of temperature in the range from 100 to 300 K. (b) Ellipticity peak amplitude changes as a function of the wave plate angle Φ, with the blue dashed and red dotted lines showing a fitting with twofold and fourfold sinusoidal functions, respectively. (c) Pump fluence dependence of the ellipticity peak amplitude of $\Delta\eta^K$ under σ_+ excitation.

independent of the helicity of the pump pulse, and it can also be induced by a linearly polarized pump beam. This suggests that the temporal relaxation slope can be assigned to the heat-induced birefringence, driven by the dynamical phenomena involving phonons. This temporal birefringence dominates the isotropic changes in the refractive index.

As shown in fig. 2(a), the differential transient polarization ellipticity $\Delta\eta^K = 1/2(\Delta\eta^K_{\sigma+} - \Delta\eta^K_{\sigma-})$ (red squares) between the σ_+ and σ_- pump beam allows us to minimize the thermal effect as the primary source of the net dichroism excited by the pump beam. In the following, we attribute this to the pure magnetic-order contribution. Figure 2(b) shows the differential polarization rotation, $\Delta\theta^K = 1/2(\Delta\theta^K_{\sigma+} - \Delta\theta^K_{\sigma-})$ (black circles), excited with opposite circularly polarized pulses. Note that the differential polarization ellipticity shows an almost Gaussian shape, while the differential polarization rotation follows the derivative shape of its ellipticity counterpart. They are related through the Kramers-Kronig relation [14].

In fig. 3(a), we present the measured peak amplitude of $\Delta\eta^K$ as a function of the temperature (red squares) pumped by circularly polarized pulses. It is important to see that the transient $\Delta\eta^K$ follows the same trend as the static magnetization curve (green circles) of the sample with decreasing temperature. The increase in the magnetization is due to the increasing long-range magnetic-order contribution [8] that occurs as the sample cools down. Based on the similar temperature dependence, it is reasonable to propose the spin origin of the observed transient photo-induced anisotropy signal.

It is instructive to compare the results in terms of the ultrafast photo-induced anisotropy for different polarizations of the pump pulse. Figure 3(b) shows the dependence of the peak amplitude of $\Delta\eta^K$ (black circles) upon the orientation of the fast axis of the quarter-wave plate relative to the polarization of the incident pump pulse, *i.e.*, the helicity of the pump pulse. The dependence can be well reproduced by a sum of twofold (blue dashed line) and fourfold (red dotted line) sinusoidal functions, which come from two main contributions: the spin-related optical orientation and the nonmagnetic, third-order nonlinear optical Kerr effect (OKE) on the ultrafast time scale, respectively [22]. It can be seen that the contribution from the optical orientation is maximized, while OKE vanishes when the pump beam is circularly polarized. It has been noted that the Kerr ellipticity induced by spin polarization only appears in the presence of the pump pulse.

It has been reported that the time scale of the spin orientation can be extracted by a simple model, which was first adapted for conventional GaAs [23] and then oxide insulators [13]. Under the assumption that both pump and probe pulses have Gaussian temporal profiles, the photo-induced polarization rotation and ellipticity can be well fitted by

$$\theta + \mathrm{i}\epsilon = A\exp\left(-\frac{t^2}{4\omega^2}\right) + B\exp\left(\frac{\omega^2}{\tau_R^2} - \frac{t}{\tau_R}\right) \times \left[1 - \mathrm{erf}\left(\frac{\omega}{\tau_R} - \frac{t}{2\omega}\right)\right],$$

where t is the pump-probe time delay and $\omega = 120$ fs is the width of the pump pulse. The erf is the Gaussian error function. A and B correspond to the symmetric and antisymmetric parts of the dielectric susceptibility tensor ε.

In the spin dynamics of semiconductors and ferromagnetic metals, the transient spin relaxation mechanism is generally consistent with the spin-orbital coupling [23]. Owing to the orbital quenching in $3d$ electron materials, we take another spin relaxation process into account. A characteristic τ_R is the Raman coherence time, which describes a transition in a degenerate state with symmetry $|+\rangle$ to $|-\rangle$, changing the magnetic quantum number and the magnetic polarization. As shown in fig. 2(b), $\tau_R = 100 \pm 30$ fs, as extracted from the fitting, which is shorter than the laser pulse duration.

To understand the photo-induced charge- and spin-related response of BFMO, we need to consider the charge transfer (CT) transitions [24]. The band gap for $BiFe_xMn_{1-x}O_3$ could be modulated from 1.2 to 2.6 eV by altering the doping ratio x between 0 and 1 [25]. Since the onset of the d-d CT transitions (~ 2 eV) in Fe^{3+}-based ferrites is strongly blue-shifted as compared to the Mn^{3+}-based manganite [24], and also the onset of the O-Mn CT transition at higher energy (~ 5 eV), the 1.55 eV pump and probe pulse used here is attributed to the intersite Mn^{3+} ion d-d transitions. The ground state of the $3d$ transition is formed by the oxygen $2p$ state, which is strongly hybridized with the $3d_3z^2$-r^2 and $3dx^2$-y^2 states. In the orthorhombic manganite BFMO, the ${}^5D$ state is split into a ${}^5\Gamma^{3+}$ low state and a ${}^5\Gamma^{5+}$ high state under the influence of a moderated crystal field of the octahedral symmetry $m3m$ [26]. Figure 1(c) shows a schematic energy-level diagram for the optical transition ($\Gamma^3 \rightarrow \Gamma^5$) between the hybridized $O^{2-}(2p)$-$Mn^{3+}(3d)$ states and the Mn^{3+} states.

The fast decay of $\Delta R/R$ corresponds to the carriers leaving the excited high state Γ^5 via electron-phonon couplings, which is characterized by the population relaxation time $\tau_1 \approx 300$ fs. The following slow process could be attributed to the carrier recombination from the upper state to the Mn-O hybrid state. The amplitude and time constant of the carrier relaxation dynamics is dependent on sample temperature. On the other hand, a circular pump pulse creates a coherent superposition of the excited states $|+\rangle$ and $|-\rangle$. Electric-dipole optical transitions from the ground state $\Gamma_3|g\rangle$ are allowed to the doubly degenerate state of symmetry state Γ_5. In the case of a circularly polarized pump pulse, it is convenient to use a circular basis for the wave functions of the doubly degenerate excited state $|+\rangle$ and $|-\rangle$, where the states $|\pm\rangle$ are characterized by the z projection J_z of the total angular momentum being equal to ± 1, respectively. The nonzero electric-dipole matrix elements for transitions from the ground state $|g\rangle$ to the excited states $|+\rangle$ and $|-\rangle$ are $\langle g|d^+|+\rangle = \langle g|d^-|-\rangle = d$, respectively. $|g\rangle, |+\rangle$ and $|-\rangle$ constitute a degenerate phenomenological three-level model, as shown in fig. 1(c). The transitions between $|+\rangle$ and $|-\rangle$ are characterized by a coherence time $\tau_R = 100 \pm 30$ fs, which could be attributed to Raman coherence and demonstrates the relaxation time of the angular momentum J_z. Furthermore, as shown in fig. 3(c), the peak magnitude of $\Delta\eta^K$ increases linearly with pump fluence, which means that the coherent superposition states are proportional to the intensity of the pump pulse, while the coherence time is independent of the pump fluence.

Conclusions. – In summary, the ultrafast photo-induced spin polarization in the multiferroic compound $BiFe_{0.5}Mn_{0.5}O_3$ has been observed on a femtosecond time scale. By means of femtosecond pump-probe transient reflectivity, Kerr rotation, and ellipticity measurements, two relaxation times are revealed. By pulse pumping, the charge transfer carriers in BFMO leave the excited state at about 300 fs by electron-lattice coupling and then recombine. With circularly polarized pulse pumping, helicity-dependent coherent spin polarization is observed. The spin polarization relaxation time is determined to be $\tau_R = 100 \pm 30$ fs, which is assigned to the Raman coherence process between the excited doubly degenerate $\Gamma^5|+,-\rangle$ state. This study provides the experimental evidence on optical orientation in $BiFe_{0.5}Mn_{0.5}O_3$ regarding ultrafast photo-induced spin polarization and paves the way to a large application potential in future spin-based all-optical technologies.

* * *

The research is supported by the National Natural Science Foundation of China (11174195), the PhD Programs Foundation of the Ministry of Education of China (20123108110003), and the Research Innovation Fund of the Shanghai Education Committee (14ZZ101) and Young Eastern Scholar (QD2015020) at Shanghai Institutions of Higher Learning. ZXC thanks the Australian Research Council for support.

REFERENCES

[1] Bibes M. and Barthélémy A., *Nat. Mater.*, **7** (2008) 425.
[2] Eerenstein E., Mathur N. D. and Scott J. F., *Nature*, **442** (2006) 759.
[3] Heron J. T., Trassin M., Ashraf K., Gajek M., He Q., Yang S. Y., Nikonov D. E., Chu Y.-H., Salahuddin S. and Ramesh R., *Phys. Rev. Lett.*, **107** (2011) 217202.
[4] Zhang J. and Li H., *Perovskite: Crystallography, Chemistry & Catalytic Performance* (Nova Science Publishers Inc. (Verlag), New York) 2013.
[5] Zhao H., Kimura H., Cheng Z., Wang X., Ozawa K. and Nishida T., *J. Appl. Phys.*, **108** (2010) 093903.
[6] Choi E.-M., Patnaik S., Weal E., Sahonta S.-L., Wang H., Bi Z., Xiong J., Blamire M. G., Jia Q. X. and MacManus-Driscoll J. L., *Appl. Phys. Lett.*, **98** (2011) 139903.
[7] Bi L., Taussig A. R., Kim H., Wang L., Dionne G. F., Bono D., Persson K., Ceder G. and Ross C. A., *Phys. Rev. B*, **78** (2008) 104106.

[8] Du Y., Cheng Z. X., Dou S. X., Wang X. L., Zhao H. Y. and Kimura H., *Appl. Phys. Lett.*, **97** (2010) 122502.
[9] Ma H., Jin Z., Zhang Z., Ma G. and Wang L., *AIP Adv.*, **2** (2012) 012116.
[10] Beck M., Metzner C., Malzer S. and Döhler G. H., *Europhys. Lett.*, **75** (2006) 597.
[11] Beaurepaire E., Merle J.-C., Daunois A. and Bigot J.-Y., *Phys. Rev. Lett.*, **76** (1996) 4250.
[12] Kirilyuk A., Kimel A. V. and Rasing Th., *Rev. Mod. Phys.*, **82** (2010) 2731.
[13] Pavlov V. V., Pisarev R. V., Gridnev V. N., Zhukov E. A., Yakovlev D. R. and Bayer M., *Phys. Rev. Lett.*, **98** (2007) 047403.
[14] Boschini F., Mansurova M., Mussler G., Kampmeier J., Grützmacher D., Braun L., Katmis F., Moodera J. S., Dallera C., Carpene E., Franz C., Czerner M., Heiliger C., Kampfrath T. and Münzenberg M., *Sci. Rep.*, **5** (2015) 15304.
[15] Jin Z., Ma H., Wang L., Ma G., Guo F. and Chen J., *Appl. Phys. Lett.*, **96** (2010) 201108.
[16] Jin Z., Ma H., Li G., Xu Y., Ma G. and Cheng Z., *Appl. Phys. Lett.*, **100** (2012) 021106.
[17] Sheu Y. M., Trugman S. A., Park Y.-S., Lee S., Yi H. T., Cheong S.-W., Jia Q. X., Taylor A. J. and Prasankumar R. P., *Appl. Phys. Lett.*, **100** (2012) 242904.
[18] Smolin S. Y., Scafetta M. D., Guglietta G. W., Baxter J. B. and May S. J., *Appl. Phys. Lett.*, **105** (2014) 022103.
[19] Talbayev D., Lee J. H., Trugman S. A., Zhang C. L., Cheong S.-W., Averitt R. D., Taylor A. J. and Prasankumar R. P., *Phys. Rev. B*, **91** (2015) 064420.
[20] Doig K. I., Peters J. J. P., Nawaz S., Walker D., Walker M., Lees M. R., Beanland R., Sanchez A. M., McConville C. F., Palkar V. R. and Lloyd-Hughes J., *Sci. Rep.*, **5** (2015) 7719.
[21] Pohl M., Pavlov V. V., Akimov I. A., Gridnev V. N., Pisarev R. V., Yakovlev D. R. and Bayer M., *Phys. Rev. B*, **88** (2013) 195112.
[22] Jin Z., Ma H., Li D., Ma G., Wang M. and Zhao C., *J. Appl. Phys.*, **109** (2011) 073109.
[23] Kimel A. V., Bentivegna F., Gridnev V. N., Pavlov V. V., Pisarev R. V. and Rasing Th., *Phys. Rev. B*, **63** (2001) 235201.
[24] Pisarev R. V., Moskvin A. S., Kalashnikova A. M. and Rasing Th., *Phys. Rev. B*, **79** (2009) 235128.
[25] Xu X. S., Ihlefeld J. F., Lee J. H., Ezekoye O. K., Vlahos E., Ramesh R., Gopalan V., Pan X. Q., Schlom D. G. and Musfeldt J. L., *Appl. Phys. Lett.*, **96** (2010) 192901.
[26] Degenhardt C., Fiebig M., Fröhlich D., Lottermoser Th. and Pisarev R. V., *Appl. Phys. B*, **73** (2001) 139.